Food & Function

Unveiling the flavone-solubilizing effects of α-glucosyl rutin and hesperidin: Probing structural differences through NMR and SAXS analyses

Journal:	*Food & Function*
Manuscript ID	FO-ART-08-2023-003261.R2
Article Type:	Paper
Date Submitted by the Author:	25-Oct-2023
Complete List of Authors:	Kadota, Kazunori; Osaka Medical and Pharmaceutical University, Pharmaceutical Sciences Kämäräinen, Tero; Osaka Medical and Pharmaceutical University Sakuma, Fumie; Chiba University Ueda, Keisuke ; Chiba University Higashi, Kenjirou; Chiba University, Graduate School of Pharmaceutical Sciences; Chiba University Moribe, Kunikazu; Chiba University, Uchiyama, Hiromasa; Osaka Medical and Pharmaceutical University, Department of Formulation Design and Pharmaceutical Technology Minoura, Katsuhiko; Osaka Medical and Pharmaceutical University Tozuka, Yuichi; Osaka Medical and Pharmaceutical University, Formulation Design and Pharmaceutical Technology

ARTICLE

Unveiling the flavone-solubilizing effects of α-glucosyl rutin and hesperidin: Probing structural differences through NMR and SAXS analyses†

Received 00th January 20xx,
Accepted 00th January 20xx

DOI: 10.1039/x0xx00000x

Kazunori Kadota,*[a] Tero Kämäräinen,[a] Fumie Sakuma,[b] Keisuke Ueda,[b] Kenjirou Higashi,[b] Kunikazu Moribe,[b] Hiromasa Uchiyama,[a] Katsuhiko Minoura[a] and Yuichi Tozuka[a]

Flavonoids often exhibit broad bioactivity but low solubility and bioavailability, limiting their practical applications. The transglycosylated materials α-glucosyl rutin (Rutin-G) and α-glucosyl hesperidin (Hsp-G) are known to enhance the dissolution of hydrophobic compounds, such as flavonoids and other polyphenols. In this study, the effects of these materials on flavone solubilization were investigated by probing their interactions with flavone in aqueous solutions. Rutin-G and Hsp-G prepared via solvent evaporation and spray-drying methods were evaluated for their ability to dissolve flavones. Rutin-G had a stronger flavone-solubilizing effect than Hsp-G in both types of composite particles. The origin of this difference in behavior was elucidated by small-angle X-ray scattering (SAXS) and nuclear magnetic resonance analyses. The different self-association structures of Rutin-G and Hsp-G were supported by SAXS analysis, which proved that Rutin-G formed polydisperse aggregates, whereas Hsp-G formed core–shell micelles. The observation of nuclear Overhauser effects (NOEs) between flavone and α-glucosyl materials suggested the existence of intermolecular hydrophobic interactions. However, flavone interacted with different regions of Rutin-G and Hsp-G. In particular, NOE correlations were observed between the protons of flavone and the α-glucosyl protons of Rutin-G. The different molecular association states of Rutin-G or Hsp-G could be responsible for their different effects on the solubility of flavone. A better understanding of the mechanism of flavone solubility enhancement via association with α-glucosyl materials would permit the application of α-glucosyl materials to the solubilization of other hydrophobic compounds including polyphenols such as flavonoids.

1. Introduction

Flavonoids are well-known biologically active, low-molecular-weight secondary metabolites produced by various plants.[1,2] More than 9,000 structural variants of flavonoids have been identified,[3,4] and a number of different flavonoids may be found in an individual species. The term flavonoid, which is derived from the Latin word *flavus* meaning yellow, originally referred to plant pigments or co-pigments.[5] All flavonoids contain a basic skeleton of 15 carbon atoms consisting of a benzene ring fused to a six-membered ring carrying a phenyl ring at the second or third position.[6] Differences in the C_3 structure present in the center of C_6-C_3-C_6 of flavan, which is the basic skeleton of aglycone, produce the various flavonoids.[7] Flavonoids are classified into six structural groups according to their hydroxylation pattern and the unsaturation degree of their skeleton.[8] In a broad sense, anthocyanin and flavanol with an anthocyanidine skeleton, are considered flavonoids. However, in a narrow sense, flavone, flavanone, and their derivatives flavanol, flavonol, and isoflavone are defined as flavonoids.

Flavonoids, which comprise the largest family of natural bioactive extracts, are formed by plants to protect against microbial invasion. For decades, flavonoids have been known as potent antioxidants based on their ability to reduce the levels of active and harmful substances, namely free radicals, via radical scavenging.[9] Flavonoids also exhibit a wide range of other functions in physiology, biochemistry, and ecology.[10,11] The physiological activity of flavonoids is believed to be based on their physical characteristics, i.e., planar structure and hydrophobicity, and their chemical characteristics, i.e., electron-donating ability of phenolic hydroxyl groups. In particular, the flavonoid structure is important because the number and position of hydroxyl groups are correlated with the activity of compounds.[12,13] Additionally, there have been many attempts to utilize flavonoids in healthy foods owing to their potential ability to protect against lung fibrosis, hepatotoxicity, and oxidative renal dysfunction.[14] However, because of their hydrophobicity, many flavonoids exhibit low solubility and bioavailability.[15,16]

To enhance the dissolution characteristics of flavonoids, various solubilization techniques have been investigated.[17] Typical methods used in the food industry to improve the solubilization of hydrophobic flavonoids include the formation of inclusion compounds with cyclodextrins[18] and micelle

[a] Faculty of Pharmacy, Osaka Medical and Pharmaceutical University, 4-20-1 Nasahara, Takatsuki, Osaka 569-1094, Japan.
[b] Graduate School of Pharmaceutical Sciences, Chiba University, 1-8-1 Inohana, Chuo-ku, Chiba 260-8675, Japan.

†Electronic Supplementary Information (ESI) available: SEM images, Powder X-ray diffraction patterns, ^{1}H NMR spectra, Rutin-G and Hsp-G SAXS analysis. See DOI: 10.1039/x0xx00000x

formation with surfactants.[19] In addition, the solubility of hydrophobic flavonoids has been successfully enhanced using solubilizing technologies based on various emulsion systems.[20–22] Recently, there has been increased interest in applying pharmaceutical technologies, such as solid dispersion and self-microemulsifying drug delivery systems, to enhance the solubility and bioavailability of hydrophobic flavonoids.[23,24] For food application, the nanocarrier formulation based on food-grade ingredients have been attracted. Nanocarrier formulations using zein, casein, glucan, and α-lactalbumin have been applied to improve the solubility of hydrophobic compounds including polyphenols.[25–29] These food-grade ingredients have mainly been used for the preparation of emulsion nanoparticles. By contrast, we developed a new solid dispersion technology using the unique properties of transglycosylated materials, including α-glucosyl hesperidin (Hsp-G) and α-glucosyl rutin (Rutin-G), to prepare formulations of hydrophobic flavonoids and transglycosylated materials with enhanced nutraceutical functions,[30–33] in addition to complexes of flavonoids with milk protein such as β-lactoglobulin, which can contribute to improvements in their functional properties.[34,35] Furthermore, the application of food-grade excipients to improve the solubility of hydrophobic compounds in nutraceuticals and supplements has been anticipated to expand the functional food market.[36,37] Hsp-G and Rutin-G are synthesized from the precursor compounds hesperidin and rutin, respectively, via transglycosylation reactions.[38–40] Several efforts have been made to clarify the underlying mechanisms by which transglycosylated materials enhance the solubility of hydrophobic compounds using nuclear magnetic resonance (NMR) and fluorescence studies.[41–43] Previous NMR studies only reported the interactions of each transglycosylated material with the targeted hydrophobic compounds in solution. However, the differences in solubilizing mechanisms for specific compounds have not been clarified. Recently, the solubilization mechanism of hydrophobic compounds via either micelles of surfactants or supramolecular self-assembly was revealed by small-angle scattering techniques.[44–47]

This study investigated the difference in the solubilizing effects of two α-glucosyl materials, namely, Rutin-G and Hsp-G, on flavone, a representative flavonoid skeleton,[41] based on the interactions of flavone with each α-glucosyl material, as determined using NMR spectroscopy. If the mechanism of solubility enhancement in flavonoids could be determined at the molecular level using NMR techniques,[48] functional food materials containing hydrophobic flavonoids could be more easily developed. We used a small-angle X-ray scattering (SAXS) technique to provide structural insights into the individual aggregation structures of Rutin-G and Hsp-G. An improved understanding of the dissolution properties of the composite particles of flavone and Rutin-G or Hsp-G is expected to broaden the applicability of α-glucosyl materials for enhancing the solubility of hydrophobic flavonoids.

2. Experimental

2.1 Materials

Flavone was purchased from Nacalai Tesque Inc. (Kyoto, Japan), Rutin-G and Hsp-G were acquired from Toyo Sugar Refining Co. (Tokyo, Japan), and commercial deuterium oxide (D_2O, 99.9%) was obtained from Sigma-Aldrich (St. Louis, MO, USA). All other chemicals and solvents were of reagent grade and used without further purification. The chemical structures and atom numbering of flavone, Hsp-G, and Rutin-G are depicted in Fig. 1.

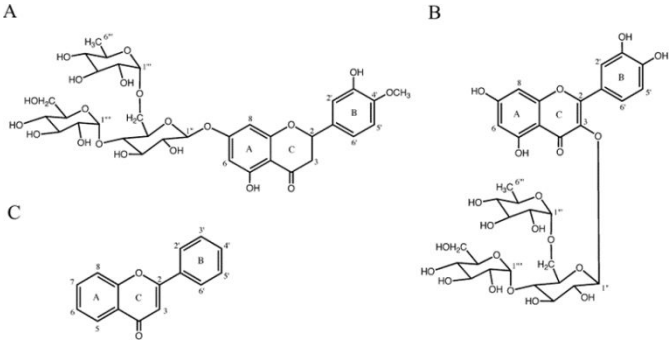

Fig. 1 Chemical structures and atom numbering of (A) α-glucosyl hesperidin (Hsp-G), (B) α-glucosyl rutin (Rutin-G), and (C) flavone.

2.2 Preparation of spray-dried particles (SDPs) and evaporated powders

SDPs and evaporated powders were prepared in references to the previous study.[30,49,50] Herein, the preparation procedures and conditions are described briefly. To prepare SDPs of flavone with Rutin-G or Hsp-G, flavone (200 mg) was dissolved in 60 mL of ethanol, and each α-glucosyl material (2000 mg) in 140 mL of distilled water. Flavone was combined with Rutin-G or Hsp-Gat at a weight ratio of 1:10 with a magnetic stirrer for 5 min at ambient temperature. The solvent of the combined mixture of flavone and α-glucosyl materials was removed using a rotary evaporator (R-3, Büchi, Flawil, Switzerland) under pressure of approximately 4 kPa in a water bath maintained at 50 °C. The obtained mixture was fed into a spray dryer (B-290, Büchi) at a rate of 8.0 mL/min. The inlet temperature of the drying chamber was set at 130 °C, resulting in the outlet temperature ranged 56–60 °C. The air flow rate for drying was approximately 35 m^3/h. Compressed air was provided distinctly to the spray nozzle at 473 L/h and 41 kPa. Physical mixtures were micronized as reference samples by grinding flavone and Rutin-G or Hsp-G together in a mortar with a pestle for 3 min. The total samples were dried in a drying cabinet under reduced pressure for one day prior to testing their physicochemical properties.

2.3 Scanning electron microscopy (SEM)

Representative SEM images of the samples were obtained using a Miniscope TM3030 instrument (Hitachi High-Technologies Co., Tokyo, Japan) at an acceleration voltage of 15 kV. Before imaging, the samples were fixed on an aluminum sample holder using double-sided carbon tape and coated with a thin layer of gold under vacuum (E-1045, Hitachi, Co. Ltd., Tokyo, Japan).

2.4 Powder X-ray diffraction (PXRD)

The total samples were evaluated using a MiniFlex powder X-ray diffractometer (Rigaku Co., Tokyo, Japan) equipped with a Cu Kα radiation source (λ = 0.15418 nm) operated at 30 kV and 15 mA. PXRD patterns were collected in the 2θ range of 5°–35° at a scanning rate of 4 °/min.

2.5 Solubility Study

The apparent solubilities of the flavone samples were measured *via* incubation for 24 h at 37 °C under shaking at 100 rpm (ML-10, Taitec, Co. Ltd., Saitama, Japan). Each flavone-containing sample (50 mg) was dispersed in 25 mL of distilled water. The amount of dissolved flavone was deduced using a high-performance liquid chromatography (HPLC) system (SPD-10A, Shimadzu Co., Ltd., Kyoto, Japan) equipped with a pump (LC-10AD), detector (SPD-10A), and column (COSMOSIL 5C18–MS-II, 4.6 mm ϕ × 150 mm; Nacalai Tesque, Inc.). The conditions were as follows: column temperature, 40 °C; wavelength, 280 nm; injection volume, 20 µL; and flow rate, 1.0 mL/min. The mobile phase was 0.1% phosphoric acid/acetonitrile (30:70, v/v).

2.6 Dissolution study

Dissolution tests were performed for the flavone samples using untreated flavone, the physical mixtures, spray-dried samples, and evaporated samples of flavone with α-glucosyl materials. The dissolution tests were completed at a paddle rotation speed of 50 rpm in a 900-mL vessel using an NTR-8000AC instrument (Toyama Sangyo, Nagoya, Japan). Each flavone-containing sample (100.0 mg) was mixed with 900 mL of distilled water at 37.0 ± 0.5 °C. The concentration of flavone in the sample was measured at 5, 10, 15, 30, 45, 60, 120, and 180 min by removing 2 mL of the solution, filtering the solution through a 0.22 µm PTFE filter, and analyzing the sample (10 µL) by HPLC, as previously described.[49]

2.7 Surface tension measurements

Surface tension was measured using the maximum bubble pressure technique with an online tensiometer (SITA Science Line t60, SITA Messtechnik GmbH, Dresden, Germany). This technique measures the dynamic surface tension at the newly formed surface of a bubble in a solution. A long bubble lifetime (1000 ms) was selected to detect low concentrations of additives under a semi-static condition. Each sample was measured under controlled conditions in triplicate at 25.0 ± 1.0 °C.

2.8 SAXS Measurements

SAXS measurements were performed using synchrotron radiation at the BL-10C of the Photon Factory (PF) in High Energy Accelerator Research Organization (KEK).[51] The measurement conditions were as follows: X-ray wavelength, 1.00 Å; temperature, 25 °C; exposure time, 240 s; beam size, 0.5 × 0.5 mm^2; camera length, 2000 mm; and detector, PILATUS2M. The samples were placed a 2-mm capillary. Other experimental procedures were similar to those applied in our previous reported papers.[42,52] The SAXS profiles were logarithmically averaged to 300 data points using Igor Pro 9.0.2.4 (WaveMetrics, Inc., Lake Oswego, OR, USA) to facilitate model fitting.[53] The analysis was performed in an arbitrary intensity scale using SASfit 0.94.11 (Paul Scherrer Institute, Villigen, Switzerland) and SasView 5.0.5 (www.sasview.org). The molecular volumes of Rutin-G and Hsp-G were estimated using CRYSOL.[54] The model details and best-fit model parameters are presented in the Supporting Information.

2.9 NMR Measurements

Using an adjustable temperature-control unit, ^{1}H NMR spectra were recorded on an Agilent DD2 600 MHz spectrometer. The ^{1}H chemical shifts were referenced to the methyl group of 3-(trimethylsilyl)propionic acid at 0 ppm at 25 °C. Sample solutions were prepared by dissolving the spray-dried samples comprising flavone and α-glucosyl materials in D_2O. Proton peak assignments were performed by combining various 2D NMR spectral techniques, including gradient correlation spectroscopy, total correlation spectroscopy, nuclear Overhauser effect spectroscopy (NOESY), gradient heteronuclear single quantum coherence, and gradient heteronuclear multiple bond correlation. NOESY spectra were measured at mixing times of 500 ms.

3. Results and Discussion

3.1 Solubility and dissolution properties of flavone with α-glucosyl materials

Using HPLC analysis, we estimated the solubility of flavone in distilled water after incubation at 37 ± 1.0 °C for 24 h to be approximately 45 µg/mL without any α-glucosyl materials. Figure 2 presents the effects of the addition of α-glucosyl materials on the amount of dissolved flavone. These experiments used physical mixtures of flavone with Rutin-G or Hsp-G prepared by dispersion in distilled water at 100 rpm. The solubility of flavone increased with increasing concentrations of the α-glucosyl materials, and its solubility was slightly higher in the presence of Rutin-G than in the presence of Hsp-G.

The powderization of hydrophobic compounds such as flavone is an in-demand process in pharmaceutical and food industries.[55] Furthermore, the microencapsulation of

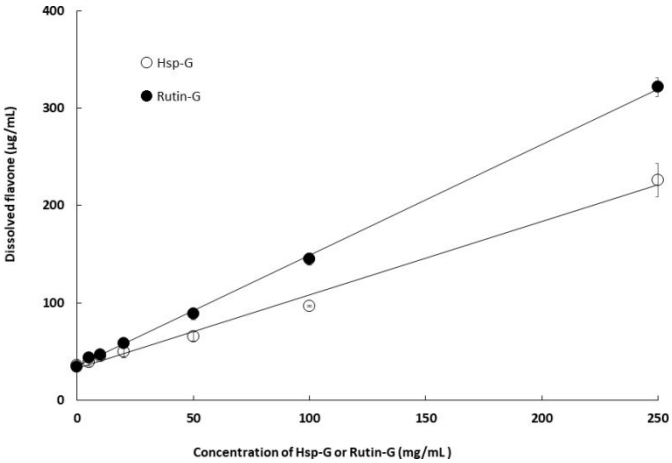

Fig. 2 Amount of dissolved flavone as a function of the loading concentration of α-glucosyl materials.

hydrophobic compounds with wall materials *via* solvent evaporation or spray drying is critical in formulating flavors in the food industry.[56] We prepared powders of flavone with α-glucosyl materials using evaporation and spray-drying methods. Previously, we improved the dissolution properties of hydrophobic compounds such as quercetin and ipriflavone with α-glucosyl materials using these methods.[31,57] The powderization of flavone with α-glucosyl materials using both methods was verified by SEM (Fig. S1).

Figure 3 presents the different dissolution patterns of untreated flavone with the spray-dried formulations, the evaporated formulations, and the physical mixtures of flavone with α-glucosyl materials. In the spray-dried, evaporated, and physical mixture formulations of flavone, both α-glucosyl materials improved the dissolution rate compared to the findings for untreated flavone. Moreover, the apparent flavone solubilities of the SDPs and evaporated powders with both α-glucosyl materials were higher than those of untreated flavone crystals. Several diffraction peaks observed in the PXRD pattern of partially treated flavone were absent in the evaporated and spray-dried formulations (Fig. S2), suggesting that flavone existed as amorphous particles or in a molecularly dispersed state in these formulations. In particular, the spray-dried formulations of flavone with the α-glucosyl materials could be considered uniformly dispersed molecular states.Although this statement were not ensured by other methods such as solid-state NMR spectroscopy in the present study, our group has previously investigated the characterization of other compounds in the Hsp-G or Rutin-G by using solid-state NMR or DSC.[50,58] Then, the compounds prepared by spray drying with α-glucosyl substances were dispersed in the molecular state. Therefore, the dissolution and release rates were highest for the spray-dried formulations containing flavone and either α-glucosyl agent, and the values peaked after 180 min. This drastic increase in the solubility of flavone could be exploited for various applications such as further processing of functional foods. Previously, we reported that the composite particles of a hydrophobic compound with α-glucosyl materials prepared by spray-drying were identified as solid dispersions,[59] indicating the promise of α-glucosyl materials as solid dispersion carriers. Similarly, the solubility of flavone differed in the presence of Hsp-G and Rutin-G. The details of this difference in flavone solubility will be discussed in the section of NMR and SAXS.

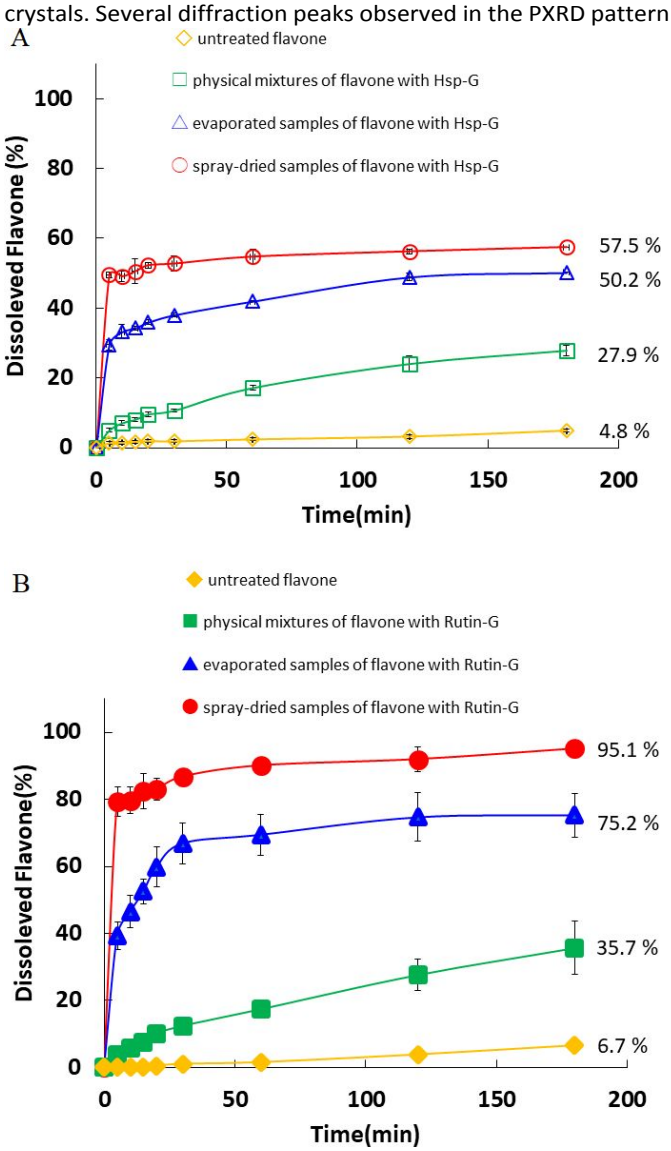

Fig. 3 Dissolution profiles of flavone (a) with Hsp-G and (b) Rutin-G in 900 mL of distilled water at 37 °C. Error bars represent the mean ± SE of three experiments.

3.2 Surface tension of α-glucosyl material solutions

We measured the surface tensions of Rutin-G or Hsp-G solutions using a maximum bubble pressure method. This measurement depends on the presence of surface-active species that can migrate and adsorb onto newly formed bubbles.[60] Figure 4 presents the relationship of the surface tensions of Rutin-G and Hsp-G solutions with the concentration of α-glucosyl materials. As previously reported, no surface activity was observed with Rutin-G even at higher concentrations,[42] whereas Hsp-G exhibited slight surface activity. The surface tension of Hsp-G solution gradually decreased as the Hsp-G concentration increased. Moreover, the surface tension changed abruptly at a specific concentration

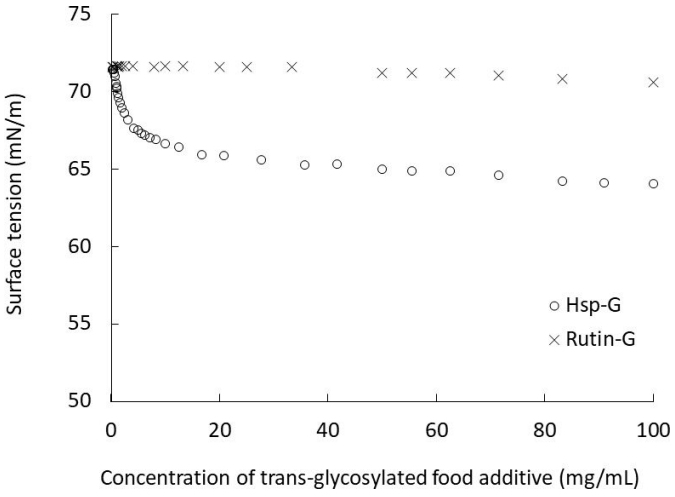

Fig. 4 Surface tension of α-glucosyl materials as a function of concentration at 25 °C.

when the interface was saturated by the adsorbed Hsp-G. The critical micelle concentration (CMC) determined from this breakpoint was approximately 5 mg/mL.[43] Normally, a small amount of surfactant with strong surface activity can enhance the solubility of compounds in water.[61] This solubilizing effect has been attributed to the micelle structures formed by the surfactants. Considering these factors, Hsp-G could more strongly enhance the solubility of flavone than Rutin-G. However, our findings revealed a discrepancy between the flavone-solubilizing effects and surface activities of the α-glucosyl materials. This behavior might be attributable to the molecular interactions of flavone with Rutin-G or Hsp-G. A similar trend was previously revealed for the solubility enhancement of ipriflavone with α-glucosyl materials,[31] with solubility being higher in the presence of Rutin-G than in the presence of Hsp-G. Furthermore, the similarities in the chemical structures of flavone and the α-glucosyl materials might have contributed to the observed improvement in flavone solubility.[30,31,41]

3.3 Rutin-G and Hsp-G association structures as determined by SAXS

SAXS is sensitive to electron density differences in the sample, which is widely used to investigate the time-averaged nano- and microstructure of many materials.[62] In SAXS, the scattering intensity, $I(q)$, is measured as a function of momentum transfer q, which is inversely related to the probed length scale. Quantitative properties of the samples are then acquired by fitting theoretical structural models to the experimental intensity profiles. We used SAXS to give insights into possible differences in the association structures of Rutin-G and Hsp-G as a function of concentration.

Up to concentrations of 15 mg/mL, the polydisperse sphere model resulted in a good fit quality for Rutin-G scattering profiles (Fig. 5A and B). At higher concentrations, the fit quality decreased drastically and further interpretation of the scattering profiles was not successful (Fig. S3 in the Supporting Information). Possible explanations for the SAXS profile shape change include increases in ellipticity and polydispersity, or

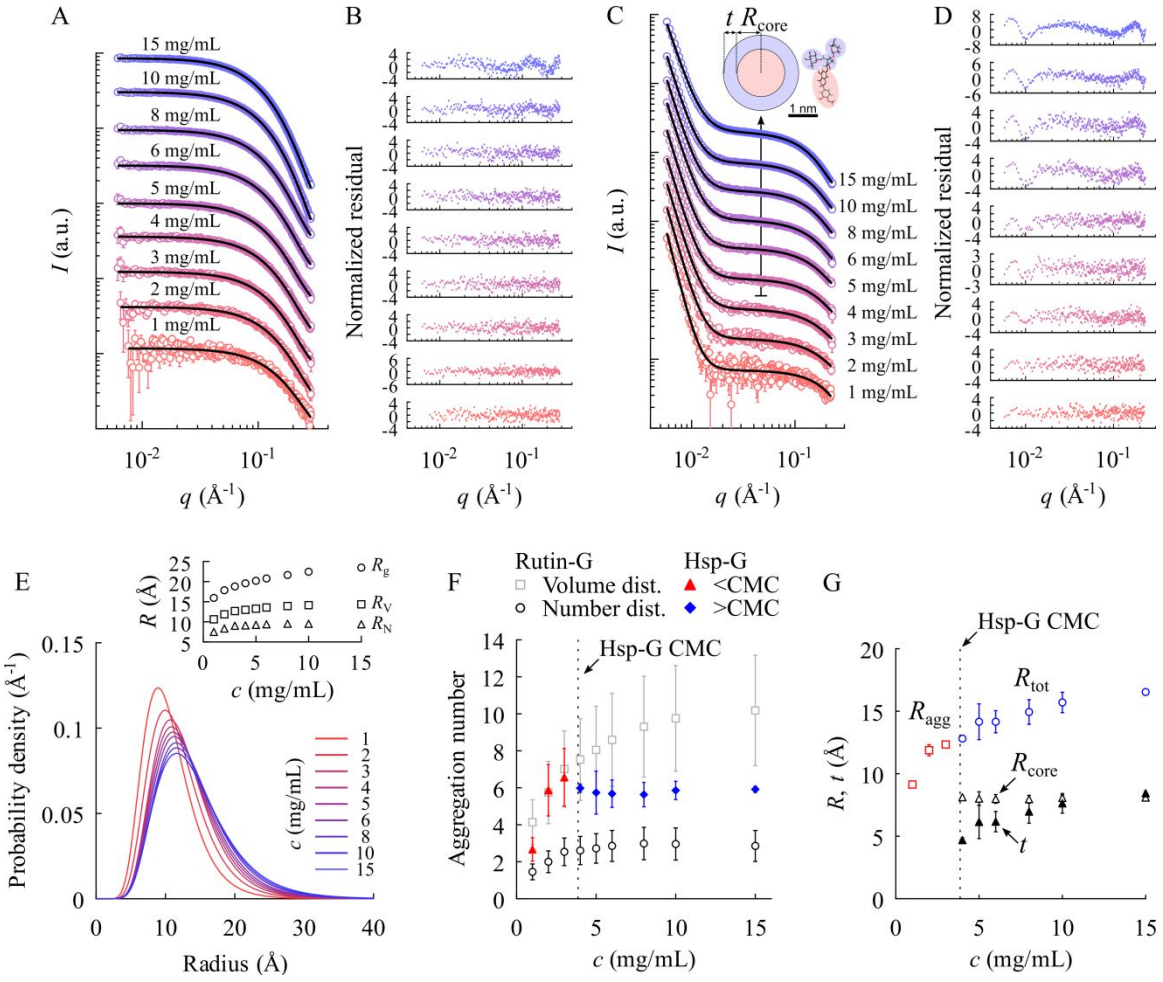

Fig 5 (A) Rutin-G and (C) Hsp-G SAXS profiles and their best-fit models (Rutin-G: polydisperse sphere model; Hsp-G: sphere model at ≤3 mg/mL, core-shell sphere model at ≥4 mg/mL) in solid lines as the concentration is varied (the data have been offset vertically for clarity), and their respective fit residuals in (B) and (D) in increasing concentration from bottom-up. In (C), the cross-section of the micelle structure corresponding to 4 mg/mL is presented in scale with Hsp-G. (E) Rutin-G aggregate volume distributions determined from SAXS analysis in the range of 1–15 mg/mL and the corresponding radius of gyration, volume-average radius (R_V), and number average radius (R_N) are shown in the inset. The number size distributions are presented in Figure S4 in the Supporting Information. (F) Volume- and number-based Rutin-G aggregation numbers. The upper and lower error bounds correspond to $N_w = 0$ and $N_w = 2$, respectively, and the Hsp-G aggregation numbers for sphere and core-shell sphere models. (G) Hsp-G premicellar aggregate radius (R_{agg}), total micelle radius ($R_{tot} = R_{core} + t$), core radius (R_{core}), and shell thickness (t) as the Hsp-G concentration varied.

structure factor effects. For Hsp-G, the monodisperse sphere model produced good fits at concentrations lower than 5 mg/mL (Figs. S4 and S5 in the Supporting Information), i.e., only slightly above the CMC of Hsp-G. Therefore, we used the CMC as a cutoff between the sphere (≤3 mg/mL) and core-shell sphere (≥4 mg/mL) models to interpret the scattering profiles. This yielded great improvement in the fit quality at concentrations up to approximately 15 mg/mL (Fig. 5C and D). Similar to the findings for Rutin-G, modeling of the scattering profiles at higher concentrations was unsuccessful.

The radius of gyration and volume average radius were more sensitive to the polydispersity of Rutin-G aggregates, which slightly increased with the concentration (Fig. 5E). Considering the number of hydroxyl groups in each Rutin-G molecule (N_{OH} = 13) and the number of water molecules associated with the hydroxyl groups of solubilized mono/disaccharides (N_w ≈ 1.5–2),[63] we estimated the Rutin-G aggregation numbers from $N_{agg} = V/(v_{Rutin\text{-}G} + N_{OH}N_w v_w)$, where V [=(4/3)πR^3] is the aggregate volume and $v_{Rutin\text{-}G}$ (940.6 Å^3) and v_w (30 Å^3) are the volumes of Rutin-G and water molecules, respectively. Between 10 and 15 mg/mL, we acquired a number distribution-based mean N_{agg} of approximately 2–4 and a volume distribution-based mean N_{agg} of approximately 7–13, where the estimated lower and (strict) upper bounds were given by the assumptions N_w = 2 and N_w = 0, respectively (Fig. 5F). Our number-based N_{agg} was in good agreement with our previous results of N_{agg} of approximately 2 below and 4 above the critical aggregation concentration (CAC) measured using ^{1}H NMR.[42] Furthermore, the number average size of Rutin-G aggregates plateaued around the previously determined CAC of 5 mg/mL.

The use of the CMC cutoff for Hsp-G gave good agreement between the models on the aggregate radius (R_{agg}) and the total size of the micelle (R_{tot}) as well as the aggregation numbers (N_{agg} ≈ 6) immediately below and above the CMC (Fig. 5F and G). The results further indicate that the growth of the micelle above the CMC is attributable to an increase in the micellar hydrophilic shell thickness (t) instead of an increase in the number of Hsp-G molecules, which would increase the radius of the hydrophobic core (R_{core}; Fig. 5G). This suggests that the conformation of the sugar moieties of Hsp-G extend slightly further out of the core, thereby enlarging the hydrocarbon corona of the micelle, as the Hsp-G concentration increased. The core-shell sphere model fit protocol used in this study was higher than the CMC that constricts the shell SLD (ρ_{shell}) based on $N_{agg} = V_{core}/v_{tail}$ and V_{shell} values (see Supporting Information), whereas the core SLD was fixed to $\rho_{core} = \rho_{tail}$. Given that no core water is present, SAXS analysis could not reject the possibility of bound water inside the micellar core because this would necessitate the fitting of ρ_{core} in addition to the arbitrary intensity scaling factor.

A spheroidal shape of the Hsp-G micelles was also supported by the packing parameter $P = v_{tail}/(A_{head}L_{tail})$, where v_{tail} (375.6 Å^3) is the tail group volume, A_{head} (given by A_{core}/N_{agg} = 140 Å^2) is the head group area on the micellar core; A_{core} is the core area, and L_{tail} (approximately 11 Å) is the length of the tail group, which yields P ≈ 0.24 within the ellipsoid range ⅓ < P < ½.[64] For Rutin-G, v_{tail} = 347.8 Å^3 and L_{tail} ≈ 5 Å given that its identical head group occupies the same area as an Hsp-G micelle and the packing parameter is much larger (P ≈ 0.50) owing to the head group conjugation site being near the center of the tail group's long axis, suggesting that Rutin-G does not readily pack into spherical structures but it tends to associate into cylindrical structures. The larger number of hydroxyl groups in the hydrophobic flavonol skeleton of Rutin-G likely acts against the micellar association, leading to spherical aggregate morphologies.

3.4 Interactions of Flavone with Rutin-G and Hsp-G by NMR

Because ^{1}H chemical shifts are sensitive to changes in the local environment of a molecule, they are often used to investigate the association state of molecules and the intermolecular interactions.[65] Furthermore, concentration-dependent ^{1}H NMR chemical shift changes and signal broadening can be used to investigate the CMC or CAC of surfactants or aggregates and the molecular mobility.[66] For example, the solution structures of the inclusion complexes of cyclodextrin with the flavonoid catechin in D_2O were revealed using NMR spectroscopy.[67] To estimate the molecular association of Hsp-G and Rutin-G at 25 °C, ^{1}H NMR spectra were measured at various concentrations (1.0–40.0 mg/mL), as presented in Fig. S6. As the observed concentration-dependent chemical shift changes of the flavanone skeleton protons of Hsp-G and the flavonoid skeleton protons of Rutin-G at 25 °C were similar to those observed in our previous studies at 37 °C,[33,49] Hsp-G and Rutin-G concentrations form micelles and aggregates, respectively, at concentrations exceeding 5 mg/mL. Hsp-G could form micelle-like structures at concentrations exceeding 5 mg/mL, as the CMC of Hsp-G determined from these chemical shift changes corresponds to that observed in the surface tension measurements. Conversely, the chemical shifts of Rutin-G changed as its concentration increased without a corresponding decrease in the surface tension, indicating that Rutin-G aggregates in solution. The CAC determined from the chemical shift dependence was 5 mg/mL, and the aggregation numbers

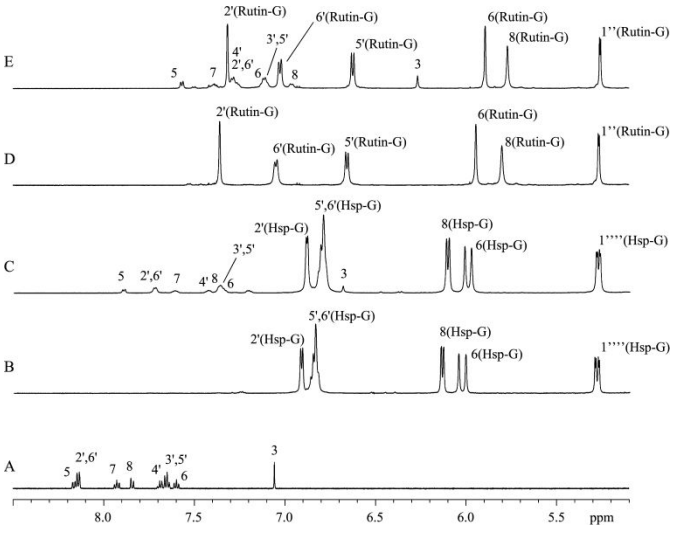

Fig. 6 ^{1}H NMR spectra of flavone (A), 20 mg/mL Hsp-G (B), 20 mg/mL flavone-loaded Hsp-G (C), 20 mg/mL Rutin-G (D), and 20 mg/mL flavone-loaded Rutin-G (E) in D_2O at 25 °C.

of Rutin-G below and above the CAC were 2 and 4, respectively, in line with the SAXS results of this work for aggregation numbers calculated from the distribution means. This result implies that small aggregates of Rutin-G form without any micelle structures, even at concentrations up to 20 mg/mL.

To determine the effects of the molecular association states of the α-glucosyl materials on the solubility improvement of flavone, the ^{1}H NMR spectra of flavone were collected in the presence and absence of 20 mg/mL Hsp-G or Rutin-G at 25 °C (Fig. 6). A comparison of the ^{1}H NMR spectra of flavone in D_2O with those of flavone in Hsp-G or Rutin-G solutions revealed that all ^{1}H signals of flavone were shifted upfield in the Hsp-G and Rutin-G solutions. These shifts were more pronounced in the Rutin-G solution, suggesting that the environment around the flavone changes greatly in the Rutin-G solution. Considering the enhancement of flavone solubility by Rutin-G compared to that by Hsp-G, Rutin-G exhibits a higher partitioning ratio of flavone into micelles compared to Hsp-G. Furthermore, each flavone ^{1}H signal was broadened in the presence of both α-glucosyl materials, suggesting that the mobility of flavone was suppressed to some extent. Furthermore, in Hsp-G and Rutin-G, the ^{1}H signals of the flavanone and flavonol skeletons exhibited upfield shifts relative to each α-glucosyl material alone without significant changes in the ^{1}H signals of the sugar moieties. These results suggested that flavone forms intermolecular

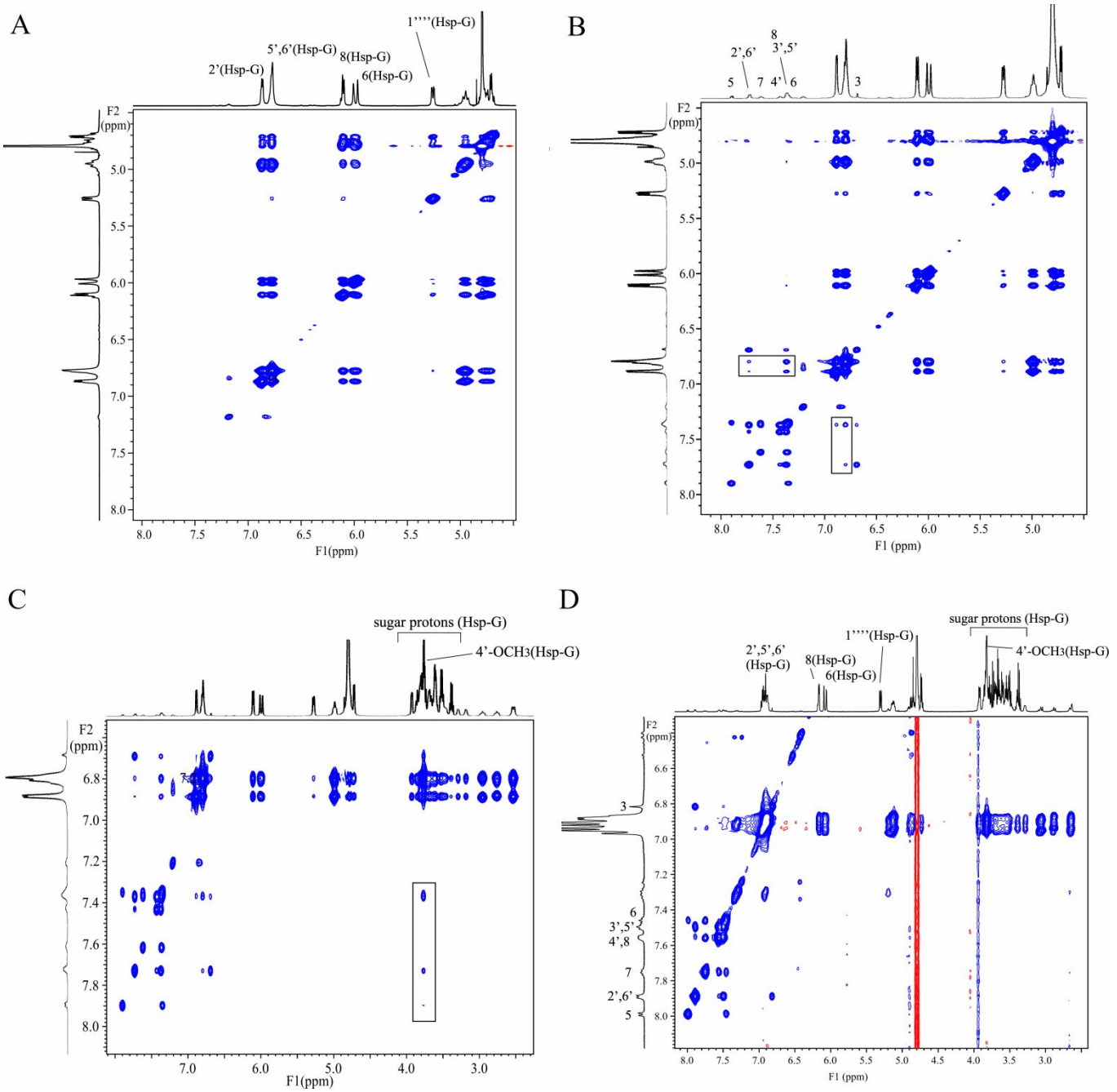

Fig. 7 Expanded regions of the NOESY spectra of 20 mg/mL Hsp-G (A), flavone-loaded 20 mg/mL Hsp-G (B, C), and flavone-loaded 5 mg/mL Hsp-G (D) in D_2O at 25 °C.

hydrophobic interactions with the flavanone skeleton of Hsp-G and the flavonol skeleton of Rutin-G.

In NOESY spectra, cross-peaks [nuclear Overhauser effects (NOEs)] are observed when the spatial distance between neighboring protons is approximately 5 Å or lower.[68,69] Therefore, this technique is useful for analyzing intermolecular interactions and three-dimensional structures. NOESY was used to investigate the location of flavone in the α-glucosyl materials. Figure 7 presents expanded regions of the NOESY spectra of Hsp-G and flavone-loaded Hsp-G in D_2O at 25 °C. The key NOE cross-peaks that can be used to deduce the possible interaction sites between flavone and Hsp-G are highlighted. As presented in Fig. 7B, NOE correlations were observed between the aromatic protons of flavone (H-2′, H-3′, H-5′, H-6′) and those of the flavanone skeleton (B ring) of Hsp-G (H-2′, H-5′, H-6′). Additionally, these flavone protons exhibited NOE cross-peaks with the 4′-OCH_3 protons of Hsp-G (Fig. 7C). These cross-peaks were not observed in the NOESY spectra of Hsp-G without flavone (Fig. 7A). These results indicate that flavone and Hsp-G form a hydrophobic intermolecular interaction between the B ring of flavone and the flavanone skeleton (B ring) of Hsp-G. Notably, these NOEs were not observed in solutions with Hsp-G concentrations of ≤5 mg/mL (Fig. 7D).

In the NOESY spectra of flavone-loaded Rutin-G, NOE correlations were observed between the hydrophobic regions of flavone and Rutin-G, as observed for flavone-loaded Hsp-G;

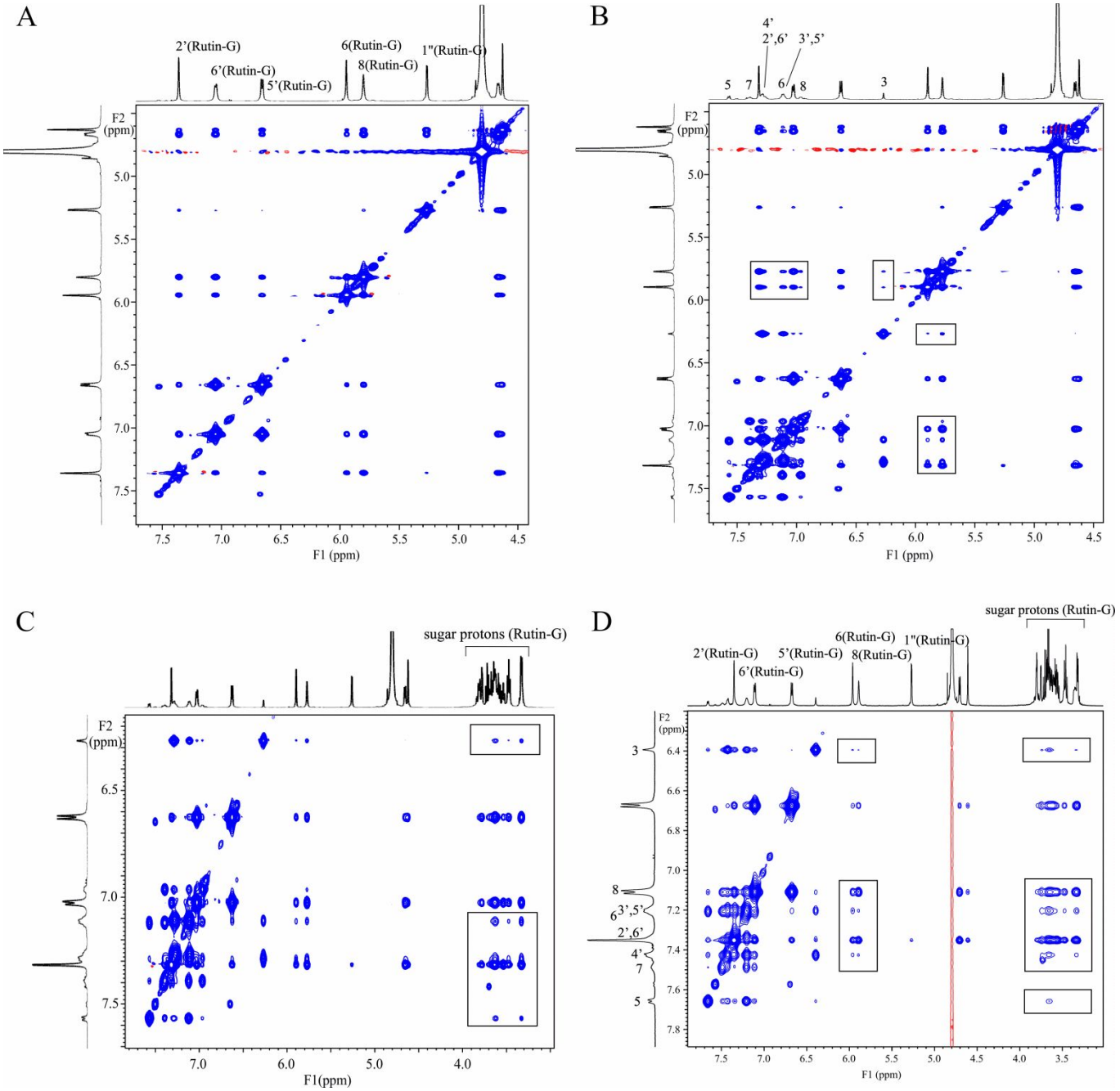

Fig. 8 Expanded regions of the NOESY spectra of 20 mg/mL Rutin-G (A), 20 mg/mL flavone-loaded Rutin-G (B, C), and 5 mg/mL flavone-loaded Rutin-G (D) in D_2O at 25 °C.

however, these NOEs were observed between the protons of flavone (H-3, H-2′, H-3′, H-5′, H-6′) and those of the flavonoid skeleton (A ring) of Rutin-G (H-6, H-8; Fig. 8B). Interestingly, these flavone protons also exhibited correlations with the α-glucosyl protons of Rutin-G (Fig. 8C). Furthermore, these NOEs were observed in the flavone-loaded 5 mg/mL Rutin-G solution (Fig. 8D). These results suggest that the interaction between flavone and Rutin-G differs from that between flavone and Hsp-G.

Finally, we can postulate the schematic illustrations of association structures of Hsp-G and Rutin-G from the results of the SAXS study. Figure 9C also presents a schematic illustration of the solubilization behavior of flavone in solutions of transglycosylated materials, as postulated from the results of the NMR study. However, we failed to obtain direct experimental support for Rutin-G and Hsp-G association structures on cryo-electron microscopy. As previously described, concentration-dependent variations in the ^{1}H chemical shifts of the flavanone skeleton protons of Hsp-G were observed. Furthermore, NOE correlations between flavone and Hsp-G were only observed in the hydrophobic regions. NMR measurements indicated that Hsp-G forms specific micelle-like aggregated structures, although these structures differ from the rigid micelle structures of conventional surfactants.[70] Thus, Hsp-G could exert a solubilizing effect on poorly water-soluble drugs via incorporation into the hydrophobic part of Hsp-G *via* hydrophobic interactions, as presented in Fig. 9A. This hypothesized solubilization mechanism for Hsp-G is supported by the absence of NOE correlations between flavone and Hsp-G at Hsp-G concentrations of <5 mg/mL (Fig. 7D). By contrast, the small aggregates observed in Rutin-G solutions at concentrations of >5 mg/mL were not micelle-like in nature, as they did not exhibit any surface activity. Specifically, the aggregated structure of Rutin-G in solution consisted of the hydrophobic part forming a core structure with the hydrophilic part partially protruding into water. Therefore, the enhancement of flavone solubilization by Rutin-G was attributed to the incorporation of flavone into the aggregates of Rutin-G, as presented in Fig. 9B. This hypothesized solubilization mechanism was supported by the results of the NMR study, as NOE correlations between flavone and Rutin-G were observed in both 5 and 20 mg/mL Rutin-G solutions in the hydrophobic region and the α-glucosyl sugar part of Rutin-G (Fig. 8D). The difference in the interaction regions between flavone and Rutin-G or Hsp-G could be responsible for the observation of different effects on solubility. This improved the understanding of the mechanism of flavone solubility enhancement by α-glucosyl materials could permit the application of α-glucosyl materials in the solubilization of other flavonoids.

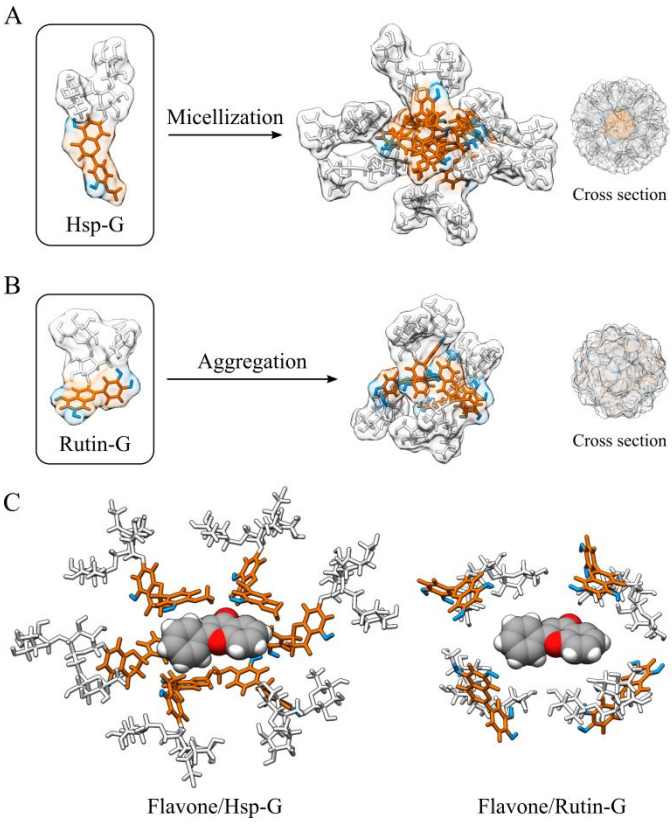

Fig. 9 Representation of (A) Hsp-G and (B) Rutin-G association structures at concentrations up to approximately 15 mg/mL and schematics depicting their time-averaged cross-sections probed with SAXS. (C) Schematic solubilization models of flavone revealed by NMR analysis in Hsp-G and Rutin-G solution.

4. Conclusions

The differences in the effects of Rutin-G and Hsp-G on flavone solubilization were investigated. Rutin-G had stronger flavone-solubilizing effects than Hsp-G when both evaporated samples and SDPs were used. This difference in the behavior of Rutin-G and Hsp-G was attributed to the molecular association states of these materials and the interactions between the transglycosylated materials and flavone in solution. From NMR and surface tension measurements, the solubilizing effect of Hsp-G on flavone was attributed to Hsp-G forming a micelle-like structure, whereas that of Rutin-G was attributed to the formation small aggregation structures in solution. The results of SAXS analysis supported the higher hydrophobic association tendency of Hsp-G, which was describable by a core-shell micelle model, whereas Rutin-G created polydisperse aggregates. The NOE correlations between Hsp-G or Rutin-G and flavone revealed interactions between the hydrophobic regions of flavone and Hsp-G or Rutin-G. Furthermore, NOE correlations were also observed between the protons of flavone and those of the α-glucosyl protons of Rutin-G. These results revealed that the mechanisms of flavone solubility enhancement by Hsp-G or Rutin-G are different. The application of α-glucosyl materials to hydrophobic flavonoids is a promising method for enhancing their dissolution properties.

Data Availability

The data that support the findings of this research are available from the corresponding author by contacting via email.

Author Contributions

Kazunori Kadota: Conceptualization, Data curation, Funding acquisition, Methodology, Project administration, Resources, Supervision, Writing – original draft. Tero Kämäräinen: Formal Analysis, Validation, Visualization, Writing – review & editing. Fumie Sakuma: Data curation, Investigation, Writing – review & editing. Keisuke Ueda: Data curation, Investigation, Writing – review & editing. Kenjirou Higashi: Data curation, Investigation, Writing – review & editing. Kunikazu Moribe: Writing – review & editing. Hiromasa Uchiyama: Writing – review & editing. Katsuhiko Minoura: Data curation, Investigation, Writing – review & editing. Yuichi Tozuka: Funding acquisition, Resources, Supervision.

Conflicts of interest

There are no conflicts to declare.

Acknowledgements

This research was partially supported by the Japan Society for the Promotion of Science (JSPS)-Joint Research Project (JPJSBP 12022942). We thank Toyo Sugar Refining Co., Ltd. for the kind gift of the α-glucosyl materials. This work benefited from the use of the SasView application, originally developed under NSF award DMR-0520547. SasView contains code developed with funding from the European Union's Horizon 2020 research and innovation programme under the SINE2020 project (grant agreement no. 654000). We are grateful to P.F. at KEK for providing the opportunity to perform SAXS experiments using synchrotron radiation.

Notes and References

1 L. A. Weston and U. Mathesius, Flavonoids: Their Structure, Biosynthesis and Role in the Rhizosphere, Including Allelopathy, *J. Chem. Ecol.*, 2013, **39**, 283–297.

2 N. Bordenave, B. R. Hamaker and M. G. Ferruzzi, Nature and consequences of non-covalent interactions between flavonoids and macronutrients in foods, *Food Funct.*, 2014, **5**, 18–34.

3 S. Martens and A. Mithöfer, Flavones and flavone synthases, *Phytochemistry*, 2005, **66**, 2399–2407.

4 H. Zhang, M. Wang, L. Chen, Y. Liu, H. Liu, H. Huo, L. Sun, X. Ren, Y. Deng and A. Qi, Structure-solubility relationships and thermodynamic aspects of solubility of some flavonoids in the solvents modeling biological media, *J. Mol. Liq.*, 2017, **225**, 439–445.

5 K. W. Bentley, The Chemistry, of Naturak Products. Volume 1: The Alkaloids, *J. Chem. Educ.*, 1958, **35**, 318.

6 M. Plaza, T. Pozzo, J. Liu, K. Z. Gulshan Ara, C. Turner and E. Nordberg Karlsson, Substituent Effects on in Vitro Antioxidizing Properties, Stability, and Solubility in Flavonoids, *J. Agric. Food Chem.*, 2014, **62**, 3321–3333.

7 C. A. Rice-Evans, N. J. Miller and G. Paganga, Structure-antioxidant activity relationships of flavonoids and phenolic acids, *Free Radic. Biol. Med.*, 1996, **20**, 933–956.

8 A. During and Y. Larondelle, The O-methylation of chrysin markedly improves its intestinal anti- inflammatory properties: Structure–activity relationships of flavone, *Biochem. Pharmacol.*, 2013, **86**, 1739–1746.

9 Y. Zhou and R. C. Tang, Natural Flavonoid-Functionalized Silk Fiber Presenting Antibacterial, Antioxidant, and UV Protection Performance, *ACS Sustain. Chem. Eng.*, 2017, **5**, 10518–10526.

10 S. L. Hwang, P. H. Shih and G. C. Yen, Neuroprotective Effects of Citrus Flavonoids, *J. Agric. Food Chem.*, 2012, **60**, 877–885.

11 M. Zhang, S. Zhu, W. Yang, Q. Huang and C. T. Ho, The biological fate and bioefficacy of citrus flavonoids: bioavailability, biotransformation, and delivery systems, *Food Funct.*, 2021, **12**, 3307–3323.

12 A. Sekher Pannala, T. S. Chan, P. J. O'Brien and C. A. Rice-Evans, Flavonoid B-Ring Chemistry and Antioxidant Activity: Fast Reaction Kinetics, *Biochem. Biophys. Res. Commun.*, 2001, **282**, 1161–1168.

13 H. J. Kim, B. L. Sang, S. K. Park, M. K. Hwan, I. P. Young and M. S. Dong, Effects of Hydroxyl Group Numbers on the B-Ring of 5,7- Dihydroxyflavones on the Differential Inhibition of Human CYP 1A and CYPIB1 Enzymes, *Arch. Pharm. Res.*, 2005, **28**, 1114–1121.

14 F. Vallejo, M. Larrosa, E. Escudero, M. P. Zafrilla, B. Cerdá, J. Boza, M. T. García-Conesa, J. C. Espín and F. A. Tomás-Barberán, Concentration and Solubility of Flavanones in Orange Beverages Affect Their Bioavailability in Humans, *J. Agric. Food Chem.*, 2010, **58**, 6516–6524.

15 K. Kadota, K. Semba, R. Shakudo, H. Sato, Y. Deki, Y. Shirakawa and Y. Tozuka, Inhibition of Photodegradation of Highly Dispersed Folic Acid Nanoparticles by the Antioxidant Effect of Transglycosylated Rutin, *J. Agric. Food Chem.*, 2016, **64**, 3062–3069.

16 K. Semba, K. Kadota, H. Arima, A. Nakanishi, M. Tandia, H. Uchiyama, K. Sugiyama and Y. Tozuka, Improved water dispersibility and photostability in folic acid nanoparticles with transglycosylated naringin using combined processes of wet-milling and freeze-drying, *Food Res. Int.*, 2019, **121**, 108–116.

17 N. Recharla, M. Riaz, S. Ko and S. Park, Novel technologies to enhance solubility of food-derived bioactive compounds: A review, *J. Funct. Foods*, 2017, **39**, 63–73.

18 N. Sali, R. Csepregi, T. Kőszegi, S. Kunsági-Máté, L. Szente and M. Poór, Complex formation of flavonoids fisetin and geraldol with β-cyclodextrins, *J. Lumin.*, 2018, **194**, 82–90.

19 T. Yin, Y. Zhang, Y. Liu, Q. Chen, Y. Fu, J. Liang, J. Zhou, X. Tang, J. Liu and M. Huo, The efficiency and mechanism of N-octyl-O, N-carboxymethyl chitosan- based micelles to enhance the oral absorption of silybin, *Int. J. Pharm.*, 2018, **536**, 231–240.

20 A. Araiza-Calahorra, M. Akhtar and A. Sarkar, Recent advances in emulsion-based delivery approaches for curcumin: From encapsulation to bioaccessibility, *Trends Food Sci. Technol.*, 2018, **71**, 155–169.

21 Z. Sebghatollahi, M. Ghanadian, P. Agarwal, H. S. Ghaheh, N. Mahato, R. Yogesh and S. H. Hejazi, Citrus Flavonoids:

Biological Activities, Implementation in Skin Health, and Topical Applications: A Review, *ACS Food Sci. Technol.*, 2022, **2**, 1417–1432.

22 Y. Lin, D. J. McClements, J. Xiao, Y. Cao and X. Liu, In Vitro−In Vivo Study of the Impact of Excipient Emulsions on the Bioavailability and Antioxidant Activity of Flavonoids: Influence of the Carrier Oil Type, *J. Agric. Food Chem.*, 2023, **71**, 1488–1498.

23 A. D. Gilley, H. C. Arca, B. L. B. Nichols, L. I. Mosquera-Giraldo, L. S. Taylor, K. J. Edgar and A. P. Neilson, Novel cellulose-based amorphous solid dispersions enhance quercetin solution concentrations in vitro, *Carbohydr. Polym.*, 2017, **157**, 86–93.

24 A. Gonçalves, N. Nikmaram, S. Roohinejad, B. N. Estevinho, F. Rocha, R. Greiner and D. J. McClements, Production, properties, and applications of solid self-emulsifying delivery systems (S-SEDS) in the food and pharmaceutical industries, *Colloids Surfaces A Physicochem. Eng. Asp.*, 2018, **538**, 108–126.

25 F. Lu, A. Mencia, L. Bi, A. Taylor, Y. Yao and H. HogenEsch, Dendrimer-like alpha-D-glucan nanoparticles activate dendritic cells and are effective vaccine adjuvants, *J. Control. Release*, 2015, **204**, 51–59.

26 S. Keshanidokht, M. A. Via, C. Y. Falco, M. P. Clausen and J. Risbo, Zein-stabilized emulsions by ethanol addition; stability and microstructure, *Food Hydrocoll.*, 2022, **133**, 107973.

27 J. B. Eun, A. Maruf, P. R. Das and S. H. Nam, A review of encapsulation of carotenoids using spray drying and freeze drying, *Crit. Rev. Food Sci. Nutr.*, 2020, **60**, 3547–3572.

28 K. Schillén, L. Galantini, G. Du, A. Del Giudice, V. Alfredsson, A. M. Carnerup, N. V. Pavel, G. Masci and B. Nyström, Block copolymers as bile salt sequestrants: intriguing structures formed in a mixture of an oppositely charged amphiphilic block copolymer and bile salt, *Phys. Chem. Chem. Phys.*, 2019, **21**, 12518–12529.

29 H. Uchiyama, M. Dowaki, K. Kadota, H. Arima, K. Sugiyama and Y. Tozuka, Single-stranded β-1,3–1,6-glucan as a carrier for improved dissolution and membrane permeation of poorly water-soluble compounds, *Carbohydr. Polym.*, 2020, **247**, 116698.

30 M. Fujimori, K. Kadota, K. Shimono, Y. Shirakawa, H. Sato and Y. Tozuka, Enhanced solubility of quercetin by forming composite particles with transglycosylated materials, *J. Food Eng.*, 2015, **149**, 248–254.

31 M. Fujimori, K. Kadota, K. Kato, Y. Seto, S. Onoue, H. Sato, H. Ueda and Y. Tozuka, Low hygroscopic spray-dried powders with trans-glycosylated food additives enhance the solubility and oral bioavailability of ipriflavon, *Food Chem.*, 2016, **190**, 1050–1055.

32 Y. Shen, Y. Xia and X. Chen, Research progress and application of enzymatic synthesis of glycosyl compounds, *Appl. Microbiol. Biotechnol.*, 2023, **107**, 5317–5328.

33 K. Kadota, M. Hashimoto, T. Yamaguchi, H. Kawachi, H. Uchiyama and Y. Tozuka, Preparation of a Highly Water-dispersible Powder Containing Hydrophobic Polyphenols Derived from Chrysanthemum Flower with Xanthine Oxidase- inhibitory Activity, *Food Sci. Technol. Res.*, 2018, **24**, 273–281.

34 M. Fu, L. Gao, Q. Geng, T. Li, T. Dai, C. Liu and J. Chen, Noncovalent interaction mechanism and functional properties of flavonoid glycoside-β-lactoglobulin complexes, *Food Funct.*, 2023, **14**, 1357–1368.

35 C. Li, T. Dai, J. Chen, X. Li, T. Li, C. Liu and D. J. McClements, Protein-polyphenol functional ingredients: The foaming properties of lactoferrin are enhanced by forming complexes with procyanidin, *Food Chem.*, 2021, **339**, 128145.

36 C. Wang, X. Chen, Y. Nakamura, C. Yu and H. Qi, Fucoxanthin activities motivate its nano/micro-encapsulation for food or nutraceutical application: a review, *Food Funct.*, 2020, **11**, 9338–9358.

37 F. Shahidi and Y. Pan, Influence of food matrix and food processing on the chemical interaction and bioaccessibility of dietary phytochemicals: A review, *Crit. Rev. Food Sci. Nutr.*, 2022, **62**, 6421–6445.

38 T. Kometani, T. Nishimura, T. Nakae, H. Takii and S. Okada, A Method for Preparation of Soluble Carthamin, Red Pigment from Safflower, Using Glycosyl Hesperidin, *Food Sci. Technol. Res.*, 1999, **5**, 265–270.

39 C. Aoki, Y. Takeuchi, K. Higashi, Y. Okamoto, A. Nakanishi, M. Tandia, J. Uzawa, K. Ueda and K. Moribe, Structural elucidation of a novel transglycosylated compound a-glucosyl rhoifolin and of a-glucosyl rutin by NMR spectroscopy, *Carbohydr. Res.*, 2017, **443–444**, 37–41.

40 R. Tang, R. Li, H. Li, X. L. Ma, P. Du, X. Y. Yu, L. Ren, L. L. Wang and W. S. Zheng, Design of Hepatic Targeted Drug Delivery Systems for Natural Products: Insights into Nomenclature Revision of Nonalcoholic Fatty Liver Disease, *ACS Nano*, 2021, **15**, 17016–17046.

41 J. Zhang, K. Higashi, K. Ueda, K. Kadota, Y. Tozuka, W. Limwikrant, K. Yamamoto and K. Moribe, Drug solubilization mechanism of α-glucosyl stevia by NMR spectroscopy, *Int. J. Pharm.*, 2014, **465**, 255–261.

42 Y. Tozuka, K. Higashi, T. Morita, M. Nishikawa, H. Uchiyama, J. Zhang, K. Moribe, K. Nishikawa, H. Takeuchi and K. Yamamoto, Transglycosylated rutin-specific non-surface-active nanostructure affects absorption enhancement of flurbiprofe, *Eur. J. Pharm. Biopharm.*, 2012, **82**, 120–6.

43 J. Zhang, Y. Tozuka, H. Uchiyama, K. Higashi, K. Moribe, H. Takeuchi and K. Yamamoto, NMR Investigation of a Novel Excipient, α-Glucosylhesperidin, as a Suitable Solubilizing Agent for Poorly Water-Soluble Drugs, *J. Pharm. Sci.*, 2011, **100**, 9–11.

44 M. Akamatsu, K. Saito, H. Iwase, T. Ogura, K. Sakai and H. Sakai, Contrast Variation Small-Angle Neutron Scattering Study of Solubilization of Perfumes in Cationic Surfactant Micelles, *Langmuir*, 2021, **37**, 10770–10775.

45 T. Kämäräinen, K. Kadota, J. Y. Tse, H. Uchiyama, T. Oguchi, H. Arima-Osonoi and Y. Tozuka, Tuning the Phytoglycogen Size and Aggregate Structure with Solvent Quality: Influence of Water−Ethanol Mixtures Revealed by X‑ray

and Light Scattering Techniques, *Biomacromolecules*, 2023, **24**, 225–237.

46 H. Takagi, T. Nakano, T. Aoki and M. Tanimoto, The structural changes of a bovine casein micelle during temperature change; in situ observation over a wide spatial scale from nano to micrometer, *Soft Matter*, 2023, **19**, 4562–4570.

47 A. Garg, S. Garg, L. J. D. Zaneveld and A. K. Singla, Chemistry and pharmacology of the Citrus bioflavonoid hesperidin, *Phyther. Res.*, 2001, **15**, 655–669.

48 H. Tang, L. Huang, C. Sun and D. Zhao, Exploring the structure–activity relationship and interaction mechanism of flavonoids and α-glucosidase based on experimental analysis and molecular docking studies, *Food Funct.*, 2020, **11**, 3332–3350.

49 K. Kadota, D. Okamoto, H. Sato, S. Onoue, S. Otsu and Y. Tozuka, Hybridization of polyvinylpyrrolidone to a binary composite of curcumin/a-glucosyl stevia improves both oral absorption and photochemical stability of curcumin, *Food Chem.*, 2016, **213**, 668–674.

50 K. Kadota, S. Otsu, M. Fujimori, H. Sato and Y. Tozuka, Soluble hydrolysis-resistant composite formulation of curcumin containing α-glucosyl hesperidin and polyvinylpyrrolidone, *Adv. Powder Technol.*, 2016, **27**, 442–447.

51 N. Shimizu, T. Mori, Y. Nagatani, H. Ohta, S. Saijo, H. Takagi, M. Takahashi, K. Yatabe, T. Kosuge and N. Igarashi, BL-10C, the small-angle x-ray scattering beamline at the photon factory, *AIP Conf. Proc.*, 2019, **2054**, 060041.

52 T. Morita, H. Okada, T. Yamada, R. Hidaka, T. Ueki, K. Niitsuma, Y. Kitazawa, M. Watanabe, K. Nishikawa and K. Higashi, A study combining magic-angle spinning NMR and small-angle X-ray scattering on the interaction in the mixture of poly(benzyl methacrylate) and ionic liquid 1-ethyl-3- methylimidazolium bis(trifluoromethanesulfonyl)amide, *Phys. Chem. Chem. Phys.*, 2022, **23**, 26575–26582.

53 J. Ilavsky and P. R. Jemian, Elucidation of the kinetic behavior of quercetin, isoquercitrin, and rutin solubility by physicochemical and thermodynamic investigations, *J. Appl. Crystallogr.*, 2009, **42**, 347–353.

54 D. Svergun, C. Barberato and M. H. Koch, PRIMUS: A Windows PC-based system for small-angle scattering data analysis, *J. Appl. Crystallogr.*, 1995, **28**, 768–773.

55 S. M. Jafari, C. Arpagaus, M. A. Cerqueira and K. Samborska, Nano spray drying of food ingredients; materials, processing and applications, *Trends Food Sci. Technol.*, 2021, **109**, 632–646.

56 H. C. F. Carneiro, R. V. Tonon, C. R. F. Grosso and M. D. Hubinger, Encapsulation efficiency and oxidative stability of flaxseed oil microencapsulated by spray drying using different combinations of wall materials, *J. Food Eng.*, 2013, **115**, 443–451.

57 H. Uchiyama, Y. Tozuka, F. Asamoto and H. Takeuchi, Fluorescence investigation of a specific structure formed by aggregation of transglycosylated stevias: Solubilizing effect of poorly water-soluble drugs, *Eur. J. Pharm. Sci.*, 2011, **43**, 71–7.

58 C. Aoki, X. Ma, K. Higashi, Y. Ishizuka, K. Ueda, K. Kadota, K. Fukuzawa, Y. Tozuka, K. Kawakami, E. Yonemochi and K. Moribe, Stabilization mechanism of amorphous carbamazepine by transglycosylated rutin, a non-polymeric amorphous additive with a high glass transition temperature, *Int. J. Pharm.*, 2021, **600**, 120491.

59 H. Sato, M. Fujimori, H. Suzuki, K. Kadota, Y. Shirakawa, S. Onoue and Y. Tozuka, Absorption improvement of tranilast by forming highly soluble nano-size composite structures associated with a-glucosyl rutin via spray drying, *Eur. J. Pharm. Biopharm.*, 2015, **92**, 49–55.

60 N. Dixit, D. L. Zeng and D. S. Kalonia, Application of maximum bubble pressure surface tensiometer to study protein–surfactant interactions, *Int. J. Pharm.*, 2012, **439**, 317–323.

61 O. A. Chat, M. H. Najar, M. A. Mir, G. M. Rather and A. A. Dar, Effects of surfactant micelles on solubilization and DPPH radical scavenging activity of Rutin, *J. Colloid Interface Sci.*, 2011, **355**, 140–149.

62 T. Kämäräinen, K. Kadota, H. Arima-Osonoi, H. Uchiyama, and Y. Tozuka, Tailoring the Self-Assembly of Steviol Glycoside Nanocarriers with Steroidal Amphiphiles, *ACS Biomater. Sci. Eng.*, 2023, **9**, 5747-5760.

63 S. A. Galema and H. Høiland, Stereochemical aspects of hydration of carbohydrates in aqueous solutions. 3. Density and ultrasound measurements, *J. Phys. Chem.*, 1991, **95**, 5321–5326.

64 J. N. Israelachvili, D. J. Mitchell and B. W. Ninham, Theory of self-assembly of hydrocarbon amphiphiles into micelles and bilayers, *J. Chem. Soc. Faraday Trans. 2 Mol. Chem. Phys.*, 1976, **72**, 1525–1568.

65 S. Ng, R. V. Sathasivam and K. M. Lo, Possible intermolecular association in triphenyltin chloride in the solution state as detected by NMR spectroscopy, *Magn. Reson. Chem.*, 2011, **49**, 749–752.

66 M. Tsianou and A. I. Fajalia, Cyclodextrins and Surfactants in Aqueous Solution above the Critical Micelle Concentration: Where Are the Cyclodextrins Located?, *Langmuir*, 2014, **30**, 13754–13764.

67 T. Ishizu, K. Kintsu and H. Yamamoto, NMR Study of the Solution Structures of the Inclusion Complexes of β-Cyclodextrin with (+)-Catechin and (-)-Epicatechin, *J. Phys. Chem. B*, 1999, **103**, 8992–8997.

68 A. W. Overhauser, Polarization of nuclei in metals, *Phys. Rev.*, 1953, **92**, 411–415.

69 J. Jeener, B. H. Meier, P. Bachmann and R. R. Ernst, Investigation of exchange processes by twodimensional NMR spectroscopy, *J. Chem. Phys.*, 1979, **71**, 4546–4553.

70 J. H. Lin, W. S. Chen and S. S. Hou, NMR Studies on Effects of Tetraalkylammonium Bromides on Micellization of Sodium Dodecylsulfate, *J. Phys. Chem. B*, 2013, **117**, 12076–12085.